

Anti-Kibble-Zurek behavior of a noisy transverse-field XY chain and its quantum simulation with two-level systems

Zhi-Peng Gao,¹ Dan-Wei Zhang,^{1,*} Yang Yu,² and Shi-Liang Zhu^{2,1,3,†}

¹*Guangdong Provincial Key Laboratory of Quantum Engineering and Quantum Materials, SPTE, South China Normal University, Guangzhou 510006, China*

²*National Laboratory of Solid State Microstructures and School of Physics, Nanjing University, Nanjing 210093, China*

³*Synergetic Innovation Center of Quantum Information and Quantum Physics, University of Science and Technology of China, Hefei, Anhui 230026, China*

(Dated: December 14, 2024)

We study the dynamics of a transverse-field XY chain driven across quantum critical points by noisy control fields. We characterize the defect density as a function of the quench time and the noise strength, and demonstrate that the defect productions for three quench protocols with different scaling exponents exhibit the anti-Kibble-Zurek behavior, whereby slower driving results in more defects. The protocols are quenching through the boundary line between paramagnetic and ferromagnetic phases, quenching across the isolated multicritical point and along the gapless line, respectively. We also show that the optimal quench time to minimize defects scales as a universal power law of the noise strength in all the three cases. Furthermore, by using quantum simulation of the quench dynamics in the spin system with well-designed Landau-Zener crossings in pseudo-momentum space, we propose an experimentally feasible scheme to test the predicted anti-Kibble-Zurek behavior of this noisy transverse-field XY chain with two-level systems under controllable fluctuations.

I. INTRODUCTION

Kibble-Zurek mechanism (KZM) provides an elegant theoretical framework for exploring the critical dynamics of phase transitions in systems ranging from cosmology to condensed matter^{1–3}. The dynamics induced by a quench across a critical point with a control parameter is generally nonadiabatic due to the critical slowing down, which results in the production of topological defects. A key prediction of KZM is that the density of defects n_0 follows a universal power law as a function of the quench time τ (transition rate $1/\tau$): $n_0 \propto \tau^{-\beta}$, where the scaling exponent $\beta > 0$ determined by the critical exponents of the phase transition and the dimensionality of the system. KZM for classical continuous phase transitions has been verified in many systems, such as cold atomic gases⁴, ion crystals^{5,6}, and superconductors⁷. There has been significant theoretical work on extension of KZM for quantum phase transitions^{8–21}, which are zero temperature transitions driven by Heisenberg quantum fluctuations rather than thermal fluctuations²². For instance, by studying KZM in the one-dimensional transverse-field Ising model, which is one of the paradigmatic models to study quantum phase transitions, it was found that the density of defects scales as the square root of the quench time with the scaling exponent $\beta = 1/2$ ^{8–10}. However, the experimental tests of KZM in quantum phase transitions are still scarce since controlling the time evolution of systems cross quantum critical points is notoriously difficult^{23–25}.

Landau-Zener transition (LZT), occurring when a two-level system sweeps through its anticrossing point, has served over decades as a textbook paradigm of quantum dynamics of some non-equilibrium physics^{26,27}. Recently, LZT has been extensively studied²⁸ both theoretically and experimentally in, e.g., superconducting qubits^{29–31},

solid-state spin systems^{32–34}, and optical lattices^{35–37}. It was shown that the dynamics of LZT can be intuitively described in terms of KZM of the topological defect formation in non-equilibrium quantum phase transition^{38,39}. The correspondence between the two physical situations provide a promising way for proof-of-concept quantum simulation of KZM in quantum regime by using LZT in two-level systems, which has been experimentally demonstrated in an optical interferometer⁴⁰. Moreover, quantum simulation of the critical dynamics in the transverse-field Ising model by a set of independent Landau-Zener crossings in pseudo-momentum space has been realized in a semiconductor electron charge qubit⁴¹, a superconducting qubit⁴² and a single trapped ion⁴³. The LZT there can be engineered well and probed with high accuracy and thus KZM of defect production in the Ising model with the scaling exponent $\beta = 1/2$ has been successfully observed in these artificial two-level systems^{41–43}.

While KZM has been verified to be broadly applicable, a conflicting observation was reported in a recent experiment of ferroelectric phase transition: slower quenches generate more defects when approaching the adiabatic limit⁴⁴. This behavior is opposite to that predicted by the standard KZM and is termed as anti-Kibble-Zurek (anti-KZ) behavior. The quench dynamics of a transverse-field Ising chain coupled to a dissipative thermal bath has been theoretically studied in Refs.^{46,47}, which show that the defect production can exhibit the anti-KZ behavior due to the emergence of thermal defects. Recently, by studying the crossing of the quantum critical point in a thermally isolated Ising chain driven by a noisy transverse field, it was demonstrated that noise contributions can also give rise to anti-KZ behavior when they dominate the dynamics⁴⁸. A natural question is

whether the anti-KZ behavior can exhibit in other quantum spin models with different scaling exponents under noisy control fields. In the experimental aspect, it would be of great value to set a stage for quantum simulation of such anti-KZ behavior in two-level systems with Landau-Zener crossings, noting that quantum spin models can only be realized in some special situations without controllable noisy fields⁵⁰⁻⁵², which may prevent the test of the anti-KZ behavior.

In this paper, we consider the dynamics of a transverse-field XY chain driven across quantum critical points by noisy control fields. We numerically calculate the defect density as a function of the quench time and the noise strength, and find that the defect productions in three quench protocols with different scaling exponents exhibit the anti-KZ behavior, i.e., slower driving results in more defects. The three protocols are quenching through the boundary line between paramagnetic and ferromagnetic phase, quenching across the isolated multicritical point and along the gapless line, which have the Kibble-Zurek scaling exponents $\beta = 1/2, 1/6, 1/3$ under the noise-free driving¹⁴⁻¹⁶, respectively. We also show that the optimal quench time to minimize defects scales as a universal power law of the noise strength in all three cases. Furthermore, by using quantum simulation of the quench dynamics in the spin system with well-designed Landau-Zener crossings, we then propose an experimentally feasible scheme to test the predicted anti-KZ behavior in this noisy transverse-field XY chain with two-level systems under controllable fluctuations in the control field. The driving protocols of the Landau-Zener crossings in two-level systems and the required parameter regions for observing the anti-KZ behavior in the three cases are presented.

The paper is organized as follows. In Section II, we illustrate that the defect productions of the transverse-field XY chain driven across quantum critical points by noisy control fields exhibit the anti-KZ behavior. In Section III, we propose to test the predicted anti-KZ behavior by using quantum simulation of the quench dynamics with well-designed LZT in two-level systems. Finally, a short conclusion is given in Sec. IV.

II. ANTI-KZ BEHAVIOR OF A NOISY TRANSVERSE-FIELD XY CHAIN

We begin with the spin-1/2 quantum XY chain under a uniform transverse field, which is one of the other exactly solvable spin models apart from the quantum Ising chain. The Hamiltonian of the transverse-field XY chain with nearest neighbor interaction is given by^{53,54}

$$H = -\frac{1}{2} \sum_{n=1}^N (J_x \sigma_n^x \sigma_{n+1}^x + J_y \sigma_n^y \sigma_{n+1}^y + h \sigma_n^z), \quad (1)$$

where N (here and hereafter we set N is even) counts the number of spins, σ_n^i ($i = x, y, z$) are the Pauli matrices

acting on the n -th spin, J_x and J_y respectively represent the anisotropy interactions along x and y spin directions, h measures the strength of the transverse field. We set $J = J_x + J_y$, $\gamma = (J_x - J_y)/J$, then the Hamiltonian can be rewritten as

$$H = -\frac{J}{2} \sum_{n=1}^N [(1 + \gamma) \sigma_n^x \sigma_{n+1}^x + (1 - \gamma) \sigma_n^y \sigma_{n+1}^y] - h \sum_{n=1}^N \sigma_n^z. \quad (2)$$

The system reduces to the isotropic XY chain for $\gamma = 0$ and the Ising chain for $\gamma = 1$. This Hamiltonian can be exactly diagonalized by using the Jordan-Wigner transformation, which maps a system of spin-1/2 to a system of spinless free fermions^{12,53,54}. The Jordan-Wigner transformation of spins to fermions is given by $\sigma_n^\pm = \exp(\pm i\pi \sum_{m=1}^{n-1} c_m^\dagger c_m)$ c_n and $\sigma_n^z = 2c_n^\dagger c_n - 1$, where $\sigma_n^\pm = \sigma_x \pm i\sigma_y$. In the fermionic language, the XY model Hamiltonian can be rewritten as

$$H = -J \sum_{l=1}^N [(c_l^\dagger c_{l+1} + c_{l+1}^\dagger c_l) + \gamma(c_l^\dagger c_{l+1}^\dagger + c_{l+1} c_l)] - h \sum_{l=1}^N (2c_l^\dagger c_l - 1). \quad (3)$$

Under the periodic boundary condition $\sigma_{N+1}^\alpha = \sigma_1^\alpha$ with even N requires that $c_{N+1} = -c_1$ and after the Fourier transformation with $c_n = \frac{e^{-i\pi/4}}{\sqrt{N}} \sum_{k \in (-\pi, \pi]} (e^{ikn} c_k)$, one can obtain $H = \sum_{k \in [0, \pi]} \Psi_k^\dagger \mathcal{H}(k) \Psi_k$, where $\Psi_k^\dagger = (c_k^\dagger, c_{-k})$ and the Hamiltonian density in the pseudomomentum space

$$\mathcal{H}(k) = -2 [\hat{\sigma}_z (J \cos k + h) + \hat{\sigma}_x (J \gamma \sin k)]. \quad (4)$$

Note that here and hereafter the Pauli matrices $\hat{\sigma}_x, \hat{\sigma}_z$ are conventionally used to write the 2×2 Hamiltonian of each independent k mode, which is distinct from the spin components σ_n^i in Eqs. (1) and (2).

The energy spectrum of the system can be obtained by diagonalizing Eq. (4), and thus the critical points or lines between different quantum phases can be found by minimizing the energy gap. Figure 1 depicts the phase diagram of the transverse-field XY chain in the space spanned by the parameters h/J and γ ¹⁴. There are a quantum paramagnetic phase denoted by PM and two ferromagnetic long-ranged phases ordering along x and y directions denoted by FMx and FMy, respectively. As shown in Fig. 1, there are three kinds of phase boundaries: an Ising critical line on the horizontal axis $\gamma = 0$ (i.e. $J_x = J_y$), a multicritical point locates at $\gamma = 0, h/J = 1$, and two gapless lines along $h/J = \pm 1$ ¹⁴⁻¹⁶. Quantum phase transition occurs when the system is driven by one or more parameters to across the boundary line or point on the phase diagram.

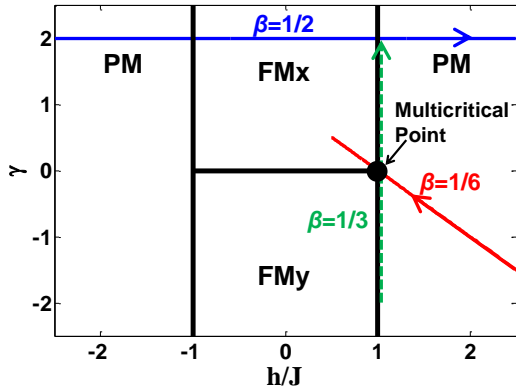


FIG. 1: (Color online) Phase diagram of the transverse-field XY chain and three quench protocols. The two vertical black solid lines separate the $\gamma - h/J$ plane into three parts. For $|h| > |J|$, the XY chain is in the paramagnetic phase denoted by PM. The middle area $|h| < |J|$ is divided into two parts (separated by horizontal black solid line at the center), which are two ferromagnetic phases denoted by FMx and FMy, ordering along x and y directions for $J_x > J_y$ and $J_x < J_y$, respectively. The horizontal blue line represents the path of the transverse quench with Kibble-Zurek scaling exponent $\beta = 1/2$. The anisotropic quench through the multicritical point (the red point) with $\beta = 1/6$ is denoted by red line across the multicritical point, and the third quench along the gapless line ($h = J$) with $\beta = 1/3$ is denoted by the green dotted line.

To study the quench dynamics of the transverse-field XY chain, we can use the Hamiltonian decoupling into a sum of independent terms $H(t) = \sum_{k \in [0, \pi]} \mathcal{H}(k, t)$, where each k -mode Hamiltonian $\mathcal{H}(k, t)$ given by Eq. (4) operates on a two-dimensional Hilbert space. The time evolution of a generic state is governed by the Schrödinger equation $i \frac{d}{dt} |\psi_k(t)\rangle = \mathcal{H}(k, t) |\psi_k(t)\rangle$. This projection of the spin Hamiltonian to the 2×2 Hilbert space has effectively reduced the quantum many-body problem to the problem of an array of decoupled two-level systems.

For the convenience of experimental implementation, we choose only one of the parameters h, J_x, J_y and γ as linearly quenched in time and the rest fixed in a specific quench protocol. As shown in Fig. 1, we consider three different quench protocols for the system driven across the phase boundaries: (1) The transverse quench with only $h(t)$ is varied in time, which is quenching through the boundary line between paramagnetic and ferromagnetic phase twice; (2) The anisotropic quench across the isolated multicritical point, in which case only the parameter $J_x(t)$ is varying and $h = 2J_y$ is set to ensure passing through the multicritical point; (3) The quench along the gapless line, which requires that $h/J = 1$ and only $\gamma(t)$ is varied. For the linear quench in the absence of dissipative thermal bath or noise fluctuations, the density of defects [see Eq. (10)] formed in three quench protocols follows the Kibble-Zurek power law as a function of the quench time with the scaling exponents

$\beta = 1/2, 1/6, 1/3^{14-16}$, respectively. In the following, we consider the three quench protocols in the transverse-field XY chain under noisy control fields and demonstrate the exhibition of anti-KZ behavior.

We now present a general framework for the description of the noise fluctuations denoted by $\eta(t)$ in the control fields. The total quench parameter is written as

$$f_j(t) = f_j^{(0)}(t) + \eta(t), \quad (5)$$

where $f_j^{(0)}(t) \propto t/\tau_j$ denote perfect control parameter linearly varying in time with quench time τ_j and the subscript $j = 1, 2, 3$ respectively represent the three quench protocols. Here $\eta(t)$ is white Gaussian noise with zero mean and the second moment $\overline{\eta(t)\eta(t')} = W^2 \delta(t - t')$, with W^2 being the strength of noise fluctuation (here η is dimensionless and W^2 has units of time). Note that white noise is a good approximation to ubiquitous colored noise with exponentially decaying correlations. We set W as a small value for the stochastic perturbation, which ensures the validity of noise-average density matrix technique⁴⁹. We consider the system Hamiltonian containing two parts in a general form⁴⁸

$$H(t) = H^{(0)}(t) + \eta(t)V, \quad (6)$$

where $H^{(0)}(t)$ denotes the ideal quench Hamiltonian to describe the evolution of the driven system, and $\eta(t)V$ denotes the fluctuation of the control fields to modified the driving progress. Defining the stochastic wave function $|\psi_\eta(t)\rangle$, the stochastic Schrödinger equation is applied to describe the interplay of these two factors (let $\hbar = 1$):

$$i \frac{d}{dt} |\psi_\eta(t)\rangle = [H^{(0)}(t) + \eta(t)V] |\psi_\eta(t)\rangle. \quad (7)$$

The stochastic density matrix is $\rho_\eta = |\psi_\eta\rangle\langle\psi_\eta|$, whose equation of motion can be derived from the dual pair of the stochastic Schrödinger equation and is given by

$$\frac{d}{dt} \rho_\eta(t) = -i[H^{(0)}(t), \rho_\eta(t)] - i[V, \eta\rho_\eta(t)]. \quad (8)$$

We then implement averaging over each realization of noise in the stochastic process. Using the Novikov's theorem⁴⁵, we have $\eta\rho_\eta(t) = -iW^2[V, \rho(t)]/2$ for the noise-averaged density matrix $\rho(t)$, and obtain the corresponding equation of motion:

$$\frac{d}{dt} \rho(t) = -i[H^{(0)}(t), \rho(t)] - \frac{W^2}{2} [V, [V, \rho(t)]], \quad (9)$$

which is directly related to the detection in realistic experiments and thus can be used to do numerical simulations of the three quench protocols under noisy control fields with the strength parameter W .

The definition of the density of defects in the transverse field XY chain after the quench is straightforward, similar to the case for the Ising model⁸⁻¹⁰. For each k -mode in a specific quench protocol, one can numerically simulate

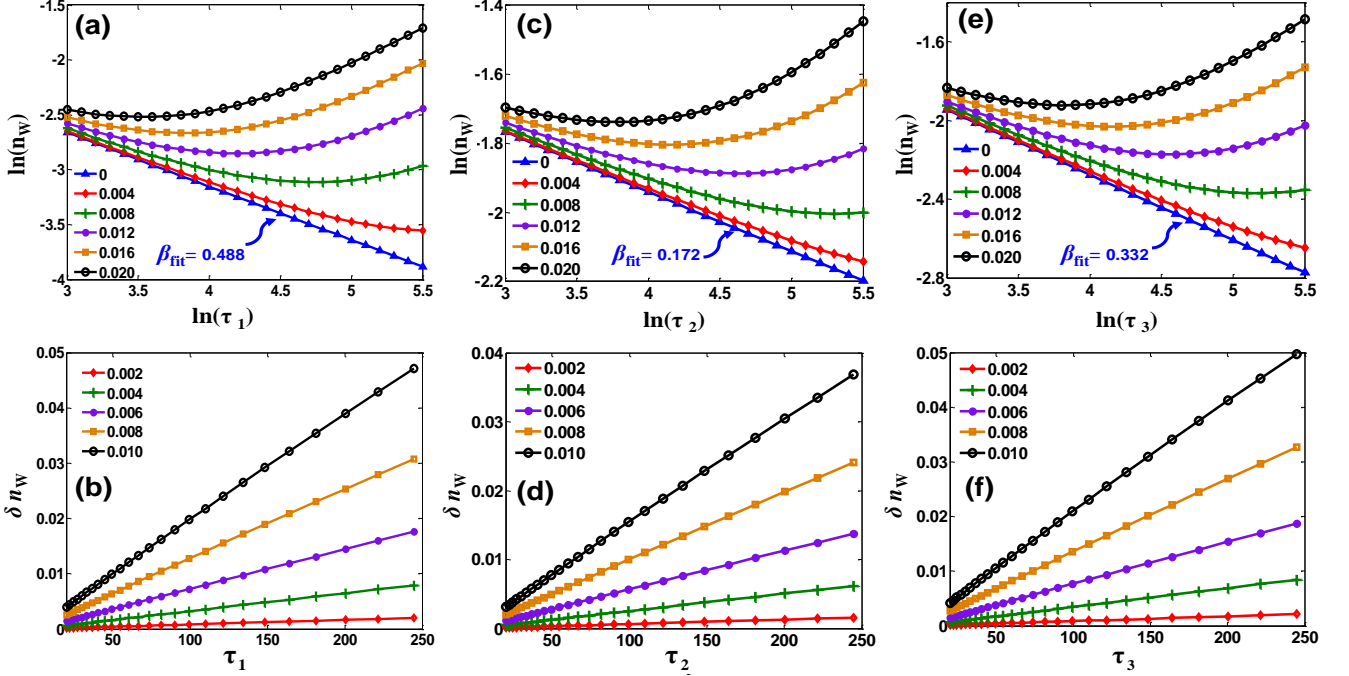


FIG. 2: (Color online) The anti-KZ behavior of the defect productions in three quench protocols. (a,c,e) For the three protocols $j = 1, 2, 3$, respectively, the defect density $n_w(\tau_j)$ as a function of the quench time for different noise strength W . (b,d,f) The corresponding noise-induced defect density $\delta n_w = n_w - n_0$ in the three cases. The quantity of W is marked by legend. The three quench protocols are the transverse quench ($j = 1$) with the linear fitting scaling exponent $\beta_{\text{fit}} = 0.488$ in the noise-free limit $W = 0$, the anisotropic quench across the multicritical point ($j = 2$) with $\beta_{\text{fit}} = 0.172$, and the quench along the gapless line ($j = 3$) with $\beta_{\text{fit}} = 0.332$. The larger W causes larger divergence from the power law prediction in KZM and the systems exhibit the anti-KZ behavior, whereby slower driving results in more defects and is remarkable in the long quench time limit.

the time evolution and find the noise-averaged density matrix $\rho_k(\tau_j)$ at the end of quench (with the quench time τ_j). In the basis of adiabatic instantaneous eigenstate $\{|G_k(\tau_j)\rangle, |E_k(\tau_j)\rangle\}$, one has $p_k = \langle E_k(\tau_j) | \rho_k(\tau_j) | E_k(\tau_j) \rangle$ to measure the probability in the excited state $|E_k(\tau_j)\rangle$ of each k -mode. For the whole XY chain, in other equivalence words, all k -modes contribute to the density of defects n_W (the subscript W denotes the presence of noises) as reasonably defined by

$$n_W = \frac{1}{N_k} \sum_{k \in [0, \pi]} p_k, \quad (10)$$

where N_k is the number of k -modes used in the summation, and it is consistent of n_0 for noise-free case with $W = 0$.

Utilizing the theoretical framework, three quench protocols can be analyzed by substituting specific $\mathcal{H}_j^{(0)}(t)$ and $V_j(t)$ into Eq. (9). We first consider the transverse quench ($j = 1$), in which case only the parameter $h(t)$ is time-dependent, as shown in Fig. 1. To describe the effect of noises in the control field h , the Hamiltonian for each k -mode $\mathcal{H}_1(k)$ can be separated into the determined

and stochastic parts as $\mathcal{H}_1(k) = \mathcal{H}_1^{(0)}(k) + V_1$, where

$$\begin{aligned} \mathcal{H}_1^{(0)}(k) &= -2[(J_x + J_y) \cos k + h(t)]\hat{\sigma}_z \\ &\quad - 2[(J_x - J_y) \sin k]\hat{\sigma}_x, \\ V_1 &= -2\hat{\sigma}_z. \end{aligned} \quad (11)$$

Here $h(t) = f_1^{(0)} = v_h t$ with the quench velocity v_h drives the system from left PM-phase region through middle FM-phase part to the right PM-phase region as shown in Fig. 1. In our numerical simulations, $h(t)$ is set to vary from $h_{\min} = -5/3$ to $h_{\max} = 5/3$, with the other two independent parameters being fixed as $J_x = 1$ and $J_y = -1/3$. For the entire process of the quench time τ_1 , we have $v_h = (h_{\max} - h_{\min})/\tau_1 = 10/(3\tau_1)$ and the whole evolution time $t \in [-\tau_1/2, \tau_1/2]$.

Figure 2(a) illustrates the numerical results of the defect density n_W as a function of the quench time τ_1 in the transverse quench protocol. When the driving field is free from noises with $W = 0$, the results of $n_0 \propto \tau_1^{-\beta_{\text{fit}}}$ with the fitting exponent $\beta_{\text{fit}} = 0.488$ agrees well with the theoretical prediction of Kibble-Zeruk scaling exponent $\beta = 1/2$ in the thermodynamical and long-time limits¹⁴⁻¹⁶. For short quench time and small noise strength, the defect density n_W as a function of the quench time τ_1 are close to the scaling form in the noise-free case. As the strength of noise fluctuation grows (in-

creasing W), the corresponding defect density increases compared to the results under noise-free condition, and the deviation becomes more significant for longer quench time, where the dynamics is dominated by the noise-induced non-adiabatic effects. Then the power-law scaling form of $n_W(\tau_1)$ fails and the system exhibits the anti-KZ behavior, i.e., slower driving (larger τ_1) results in more defects. Finally n_W is completely governed by the anti-KZ contribution in the limit of very long quench time.

We proceed to consider the second quench protocol ($j = 2$), the anisotropic quench across the multicritical point with the control field $J_x(t)$ and fixed $h = 2J_y$, as shown in Fig. 1. In this case, the Hamiltonian for each k -mode can be written as $\mathcal{H}_2(k) = \mathcal{H}_2^{(0)}(k) + V_2$, where

$$\begin{aligned} \mathcal{H}_2^{(0)}(k) &= -2\{[J_x(t) + J_y]\cos(k) + h\}\hat{\sigma}_z \\ &\quad -2[(J_x(t) - J_y)\sin(k)]\hat{\sigma}_x, \\ V_2 &= -2[(\sin k)\hat{\sigma}_x + (\cos k)\hat{\sigma}_z]. \end{aligned} \quad (12)$$

Here the linearly driving field $J_x(t) = f_2^{(0)}(t) = v_x t$ with the quench velocity v_x . Similar to the first protocol mentioned above, in our numerical simulations, we choose $h = 2$ and $J_y = 1$, and let J_x ramp from -1 to 3 with the overall ramp time τ_2 . Under this condition, the system is initially in the PM phase and then driven through the multicritical point into the FMx phase. Consequently, the quench velocity $v_x = 4/\tau_2$, and the evolution progress is $t \in [-\tau_2/4, 3\tau_2/4]$. Figure 2(c) shows the numerical results of the defect density $n_W(\tau_2)$ in this quench protocol. In the noise-free limit with $W = 0$, we find that $n_0 \propto \tau_1^{-\beta_{\text{fit}}}$ with the fitting exponent $\beta_{\text{fit}} = 0.172$ agrees with the theoretical prediction $\beta = 1/6^{14-16}$. When the dynamics is dominated by the noise effects for increasing the noise strength and (or) quench time, this power-law scaling again fails and the system exhibits similar anti-KZ behavior.

For the last quench protocol along the gapless line protocol ($j = 3$), the parameter $\gamma = f_3^{(0)} = (J_x - J_y)/J$ is used as the control field to linearly drive the system, which takes the form $\gamma(t) = v_\gamma t = (4/\tau_3)t$ in the evolution progress $t \in [-\tau_3/2, \tau_3/2]$. The other parameters are set as $h = J = J_x + J_y = 1$. Therefore, the Hamiltonian for each k -mode in this case is $\mathcal{H}_3(k) = \mathcal{H}_3^{(0)}(k) + V_3$, where the two parts

$$\begin{aligned} \mathcal{H}_3^{(0)}(k) &= -2[(J \cos k + h)\hat{\sigma}_z + J\gamma(t) \sin k \hat{\sigma}_x], \\ V_3 &= -2J \sin k \hat{\sigma}_x. \end{aligned} \quad (13)$$

The numerical results of the defect density $n_W(\tau_3)$ in this quench protocol are shown in Fig. 2(e). For $W = 0$, we find that $n_0 \propto \tau_1^{-\beta_{\text{fit}}}$ with the fitting scaling exponent $\beta_{\text{fit}} = 0.332$ consistent with the theoretical prediction $\beta = 1/3^{14-16}$. Increasing the noise strength W , the system enters the anti-KZ regime, with more defects formed for longer quench time. Hence, we come to the conclusion that when the noises presents in the control fields, the

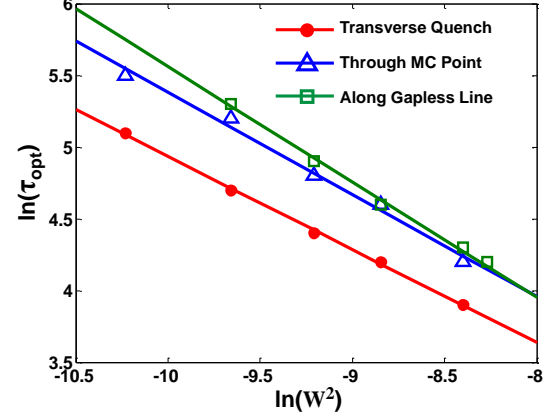


FIG. 3: (Color online) The optimal quench time τ_{opt} to minimize defects scales as a power law of the noise strength in the three quench protocols. $\ln(\tau_{\text{opt}})$ as a function of $\ln(W^2)$ with linear fitting gives $\ln(\tau_{\text{opt}}) \propto \alpha_{\text{fit}} \ln(W^2)$, where the fitting parameters for the three cases are given by: $\alpha_{\text{fit}} = -0.6496$ for the transverse quench, which is close to analytical result $\alpha = -2/3 = -0.6667$; $\alpha_{\text{fit}} = -0.8055$ for the quench through the multicritical point with $\alpha = -6/7 = -0.8571$; $\alpha_{\text{fit}} = -0.71196$ for the quench along gapless line with $\alpha = -3/4 = -0.75$.

anti-KZ behavior exists in all the three quench protocols in the transverse-field XY chain with different noise-free Kibble-Zeruk scaling exponents.

Due to the exhibition of the anti-KZ behavior in the quench when the noise presents, it is imperative to find an optimal quench time τ_{opt} to minimize the defects. Under the condition of finite quench time τ_j , the optimal control in the annealing of quantum simulator give a challenge that defect (excitation) density is produced as less as possible. For our numerical results, we focus on the region $3.0 \leq \ln(\tau_j) \leq 5.5$, since the experimental systems only maintain their quantum coherent characteristic in finite ramp time. First, as the defect density in the absence of noises $n_0 \approx c\tau_j^{-\beta}$ with the prefactor c being predicted by KZM, we can define

$$\delta n = n_W - n_0 \approx n_W - c\tau_j^{-\beta} \quad (14)$$

to characterize the noise-induced defect density. Figure 2(b,d,f) display that δn for the three quench protocols ($j = 1, 2, 3$) is almost linearly depend on τ_j when $W \ll 1$, and thus one has

$$\delta n \approx r\tau_j, \quad (15)$$

with r being the coefficient whose value depends on the noise strength. Secondly, the optimal quench time τ_{opt} can be derived approximately by minimizing δn in Eq. (14), which is then given by⁴⁸

$$\tau_{\text{opt}} \propto r^{-1/(\beta+1)} = r^\alpha. \quad (16)$$

This relation is verified to be applicable for all the three quench protocols in the parameter regions we considered,

as illustrated in Fig. 3. In the original KZM scenario, only the control fields without noises accounts for the production of defect and long quench time τ_j prevents defects formation. However, we have shown that the noises in the control fields, which is a more practical situation in realistic experiments, can also induce defects and it is intuitively to use shorter quench time as optimum to suppress the defect production when noise strength W gets larger.

III. QUANTUM SIMULATION OF THE ANTI-KZ BEHAVIOR IN TWO-LEVEL SYSTEMS

In this section, we propose to test the predicted anti-KZ behavior by quantum simulation of the quench dynamics with LZT in two-level systems. We first present a method to transform a generic two-level Hamiltonian with time linearly dependent term in the diagonal term into a standard LZT form. In a two-level system, the Schrödinger equation for the state vector $|\psi(t)\rangle = u_1(t)|e\rangle + u_2(t)|g\rangle$ with $|e\rangle$ and $|g\rangle$ as the diabatic basis can be written as

$$i \frac{d}{dt} \begin{pmatrix} u_1 \\ u_2 \end{pmatrix} = -2 \begin{pmatrix} vt + C & \Delta \\ \Delta & -vt - C \end{pmatrix} \begin{pmatrix} u_1 \\ u_2 \end{pmatrix}. \quad (17)$$

Here we assume the parameters v, Δ and C are real constants. We further use the substitution

$$\begin{aligned} v_{LZ} &= v/(2\Delta)^2 \\ t_{LZ} &= 4\Delta(t + C/v) \end{aligned} \quad (18)$$

into the origin two-level system Hamiltonian (17), which can then be transformed into the standard LZT form,

$$i \frac{d}{dt_{LZ}} \begin{pmatrix} u_1 \\ u_2 \end{pmatrix} = -\frac{1}{2} \begin{pmatrix} v_{LZ}t_{LZ} & 1 \\ 1 & -v_{LZ}t_{LZ} \end{pmatrix} \begin{pmatrix} u_1 \\ u_2 \end{pmatrix}. \quad (19)$$

The probability in the excited state at the end of the driving is approximately given by the Landau-Zener formula $P_{LZ} = \exp(-\frac{2\pi\Delta^2}{v})^{26-28}$.

On the other hand, KZM can be used to study the dynamics in the quantum phase transition driven across the quantum critical point. The essence of KZM is the adiabatic impulse approximation³⁸, where the quench process is divided into three stages: adiabatic far away from the critical point, frozen state in the vicinity of the point when $[-\hat{t}, \hat{t}]$ with \hat{t} denoting the freeze-out time scale, and the restart of adiabatic process. For convention, we define the relaxation time as $\tau_{\text{rel}} = g^{-1}$, where g is the energy gap between the ground state and the first excited state, and \hat{t} is estimated with $\tau_{\text{rel}} = \alpha\hat{t}$ and $\alpha = \mathcal{O}(1)$. Let $\alpha = 1$, the impulse region is given by $(-v_{LZ}^{-1}, v_{LZ}^{-1})^9$. When the starting and ending points of t_{LZ} in the Landau-Zener Hamiltonian is outside the impulse region, it can be regarded that there is a complete LZT in this two-level system. The similarity between LZT and KZM was firstly point out in³⁸, one of the most

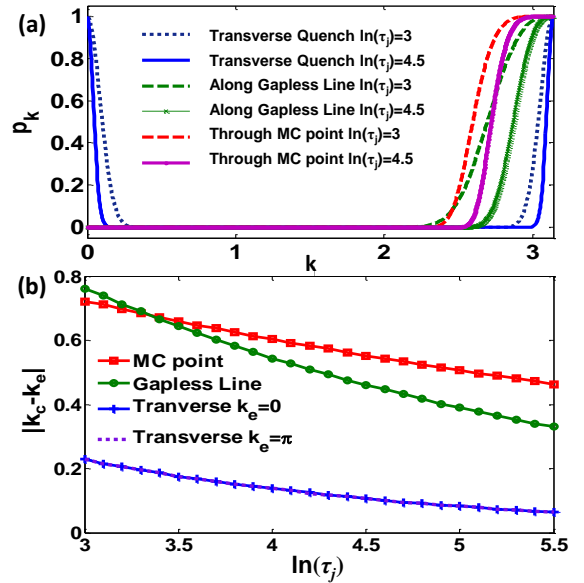


FIG. 4: (Color online) (a) The excitation probability p_k as a function of k . In the transverse quench ($j = 1$), the regions with major contribution are near the points $k_e = 0, \pi$, while near $k_e = \pi$ in the quench through the multicritical point ($j = 2$) and along gapless line ($j = 3$). (b) The relative length of the suggested simulation regions (see the text) $|k_c - k_e|$ as a function of $\ln(\tau_j)$, where the cutoff k_c is determined by the excitation probability $p_k(k) > 0.03$.

prominent features is that when the system approaches the critical point, the inverse of the energy gap tends to infinity in KZM and the counterpart in LZT also increases.

The defect density n_W can also be estimated by the integral of the transition probability $P_{LZ} \approx p_k$ over the pseudo-momentum space⁴¹⁻⁴³

$$n_W \approx \frac{1}{\pi} \int_0^\pi P_{LZ}(k) dk, \quad (20)$$

which can be measured in two-level systems by means of quantum simulation of the quench dynamics with well-designed Landau-Zener crossings, similar as the experiments for the Ising chain without noises⁴¹⁻⁴³. For the three quench protocols in the noisy XY chain, the parameters in (17) for a two-level system correspond to the counterparts in the Hamiltonian of the noise-free quench $\mathcal{H}_j^{(0)}(k)$ ($j = 1, 2, 3$ for the three protocols). In addition, the noise part $\eta(t)V_j$ correspond to stochastic fluctuations of the control fields V_j , which can be realized by inducing the $\hat{\sigma}_z$ or (and) $\hat{\sigma}_x$ fluctuations with tunable strength W into the two-level systems.

To simulate the transverse quench ($j = 1$) in transverse field XY chain with many independent LZT in pseudo-momentum space, one can use the mapping $v \rightarrow v_h, \Delta \rightarrow (J_x - J_y) \sin k$ and $C \rightarrow (J_x + J_y) \cos k$. This indicates

the substitution in this quench protocol

$$\begin{aligned} v_{LZ} &= v_h/(2J\gamma \sin k)^2 \\ t_{LZ} &= 4J\gamma \sin k(t + J \cos k/v_h), \end{aligned} \quad (21)$$

which can transform $\mathcal{H}_1(k)$ into the standard LZT form. For the second quench protocol ($j = 2$) of anisotropic quench through the multicritical point, following the mapping of the parameters similar as those in the first case, one can obtain the corresponding substitution

$$\begin{aligned} v_{LZ} &= v_x/[2(J_y \sin 2k + h \sin k)]^2 \\ t_{LZ} &= 4(J_y \sin 2k + h \sin k) \\ &[t + (J_y \cos 2k + h \cos k)/v_x]. \end{aligned} \quad (22)$$

Similarly, for the third quench protocol ($j = 3$) along the gapless line, the mapping of the Hamiltonian in pseudo-momentum space gives the corresponding substitution

$$\begin{aligned} v_{LZ} &= v_\gamma \sin k/[2(\cos k + 1)]^2 \\ t_{LZ} &= -4(\cos k + 1)t. \end{aligned} \quad (23)$$

To reduce the number of implementing LZT in the estimation of the predicted n_W , we consider the distribution of the excitation probability p_k as a function of k . The results for the three protocols with typical quench time τ_j are plotted in Fig. 4(a). One can find that only those k modes in the regions near the points $k_e = 0$ and (or) $k_e = \pi$ contribute the major to the excitation formation. Therefore in experiments, one can just implement some LZT of the k modes in these regions to extract the simulated defect density. For practical implementation, one may define a cutoff pseudo-momentum k_c in quantum simulation, which separates the k axis into two or three

(for transverse quench) parts determined by the excitation probability $p_k(k) > 0.03$ here (other small values are also applicable). Figure 4(b) depicts $|k_c - k_e|$ as a function of the quench time in the three protocols, which approximately gives the length of the required simulation regions measured from the point k_e . The results also show that the region length monotonously decreases as increasing τ_j .

IV. CONCLUSIONS

In summary, we have studied the quench dynamics of a transverse-field XY chain driven across quantum critical points by noisy control fields and demonstrated that the defect productions for three quench protocols with different scaling exponents exhibit the anti-KZ behavior. We have also shown that the optimal quench time to minimize defects scales as a universal power law of the noise strength for all the three cases. Moreover, by using quantum simulation of the quench dynamics in the spin system with well-designed Landau-Zener crossings in pseudo-momentum space, we have proposed an experimentally feasible scheme to test the predicted anti-KZ behavior.

Acknowledgments

This work was supported by the NSFC (Grants No. 11604103, No. 11474153, and No. 91636218), the NKRDP of China (Grant No. 2016YFA0301803), the NSF of Guangdong Province (Grant No. 2016A030313436), and the Startup Foundation of SCNU.

* Electronic address: zdanwei@126.com

† Electronic address: slzhu@nju.edu.cn

¹ T. W. B. Kibble, Topology of cosmic domains and strings, *J. Phys. A* **9**, 1387 (1976).

² W. H. Zurek, Cosmological experiments in superfluid helium, *Nature* **317**, 505 (1985).

³ W. H. Zurek, Cosmological experiments in condensed matter systems, *Phys. Rep.* **276**, 177 (1996).

⁴ N. Navon, A.L. Gaunt, R.P. Smith, and Z. Hadzibabic, Critical dynamics of spontaneous symmetry breaking in a homogeneous Bose gas, *Science* **347**, 167 (2015).

⁵ S. Ulm, J. Roßnagel, G. Jacob, C. Degnther, S. T. Dawkins, U. G. Poschinger, R. Nigmatullin, A. Retzker, M. B. Plenio, F. Schmidt-Kaler, and K. Singer, Observation of the Kibble-Zurek scaling law for defect formation in ion crystals, *Nat. Commun.* **4**, 2290 (2013).

⁶ K. Pyka, J. Keller, H. L. Partner, R. Nigmatullin, T. Burgermeister, D. M. Meier, K. Kuhlmann, A. Retzker, and M. B. Plenio, Topological defect formation and spontaneous symmetry breaking in ion Coulomb crystals, *Nat. Commun.* **4**, 2291 (2013).

⁷ R. Monaco, J. Mygind, and R. J. Rivers, Zurek-Kibble

Domain Structures: The Dynamics of Spontaneous Vortex Formation in Annular Josephson Tunnel Junctions, *Phys. Rev. Lett.* **89**, 080603 (2002).

⁸ J. Dziarmaga, Dynamics of a quantum phase transition and relaxation to a steady state, *Adv. Phys.* **59**, 1063 (2010).

⁹ J. Dziarmaga, Dynamics of a quantum phase transition: Exact solution of the quantum Ising model, *Phys. Rev. Lett.* **95**, 245701 (2005).

¹⁰ W. H. Zurek, U. Dorner, and P. Zoller, Dynamics of a quantum phase transition, *Phys. Rev. Lett.* **95**, 105701 (2005).

¹¹ J. Dziarmaga, Dynamics of a quantum phase transition in the random Ising model: logarithmic dependence of the defect density on the transition rate, *Phys. Rev. B* **74**, 064416 (2006).

¹² T. Caneva, R. Fazio, and G. E. Santoro, Adiabatic quantum dynamics of a random Ising chain across its quantum critical point, *Phys. Rev. B* **76**, 144427 (2007).

¹³ D. Patan, A. Silva, L. Amico, R. Fazio, and G. E. Santoro, Adiabatic dynamics in open quantum critical many-body systems, *Phys. Rev. Lett.* **101**, 175701 (2008).

¹⁴ V. Mukherjee, U. Divakaran, A. Dutta, and D. Sen, Quenching dynamics of a quantum XY spin-1/2 chain in a transverse field, *Phys. Rev. B* **76**, 174303 (2007).

¹⁵ U. Divakaran, V. Mukherjee, A. Dutta, and D. Sen, Defect production due to quenching through a multicritical point, *J. Stat. Mech.* P02007 (2009).

¹⁶ U. Divakaran, A. Dutta, and D. Sen, Quenching along a gapless line: A different exponent for defect density, *Phys. Rev. B* **78**, 144301 (2008).

¹⁷ S. Deng, G. Ortiz, and L. Viola, Dynamical non-ergodic scaling in continuous finite-order quantum phase transitions, *Eurphys. Lett.* **84**, 67008 (2009).

¹⁸ J. Sabbatini, W. H. Zurek, and M. J. Davis, Phase Separation and Pattern Formation in a Binary Bose-Einstein Condensate, *Phys. Rev. Lett.* **107**, 230402 (2011).

¹⁹ M. Kolodrubetz, B. K. Clark, and D. A. Huse, Nonequilibrium Dynamic Critical Scaling of the Quantum Ising Chain, *Phys. Rev. Lett.* **109**, 015701 (2012).

²⁰ T. Caneva, R. Fazio, and G. E. Santoro, Adiabatic quantum dynamics of the Lipkin-Meshkov-Glick model, *Phys. Rev. B* **78**, 104426 (2008).

²¹ O. L. Acevedo, L. Quiroga, F. J. Rodriguez, and N. F. Johnson, New dynamical scaling universality for quantum networks across adiabatic quantum phase transitions, *Phys. Rev. Lett.* **112**, 030403 (2014).

²² S. Sachdev, *Quantum Phase Transitions* (Cambridge University Press, Cambridge, England, 1999).

²³ D. Chen, M. White, C. Borries, and B. DeMarco, Quantum Quench of an Atomic Mott Insulator, *Phys. Rev. Lett.* **106**, 235304 (2011).

²⁴ S. Braun, M. Friesdorf, S. S. Hodgman, M. Schreiber, J. P. Ronzheimer, A. Riera, M. del Rey, I. Bloch, J. Eisert, and U. Schneider, Emergence of coherence and the dynamics of quantum phase transitions, *Proc. Natl. Acad. Sci.* **112**, 3641 (2015).

²⁵ M. Anquez, B. A. Robbins, H.M Bharath, M. Boguslawski, T. M. Hoang, and M. S. Chapman, Quantum Kibble-Zurek Mechanism in a Spin-1 Bose-Einstein Condensate, *Phys. Rev. Lett.* **116**, 155301 (2016).

²⁶ L. D. Landau, On the theory of transfer of energy at collisions II. *Physik. Z. Sowjet.* **2**, 46 (1932).

²⁷ C. Zener, Non-adiabatic crossing of energy levels. *Proc. R. Soc. London, Ser. A* **137**, 696 (1932).

²⁸ S. N. Shevchenko, S. Ashhab, and F. Nori, Landau-Zener-Stückelberg interferometry. *Phys. Rep.* **492**, 1 (2010).

²⁹ W. D. Oliver, Y. Yu, J. C. Lee, K. K. Berggren, L. S. Levitov, and T. P. Orlando, Mach-Zehnder interferometry in a strongly driven superconducting qubit. *Science* **310**, 1653 (2005).

³⁰ M. Sillanpaa, T. Lehtinen, A. Paila, Y. Makhlin, and P. Hakonen, Continuous-time monitoring of Landau-Zener interference in a cooper-pair box. *Phys. Rev. Lett.* **96**, 187002 (2006).

³¹ X. Tan, D.-W. Zhang, Z. Zhang, Y. Yu, S. Han, and S.-L. Zhu, Demonstration of Geometric Landau-Zener Interferometry in a Superconducting Qubit. *Phys. Rev. Lett.* **112**, 027001 (2014).

³² J. R. Petta, H. Lu, and A. C. Gossard, A Coherent Beam Splitter for Electronic Spin States, *Science* **327**, 669 (2010).

³³ C. Betthausen, T. Dollinger, H. Saarikoski, V. Kolkovsky, G. Karczewski, T. Wojtowicz, K. Richter, and D. Weiss, Spin-transistor action via tunable Landau-Zener transitions, *Science* **337**, 324 (2012).

³⁴ G. Cao, H.-O. Li, T. Tu, L. Wang, C. Zhou, M. Xiao, G.-C. Guo, and H.-W. Jiang, Ultrafast universal quantum control of a quantum-dot charge qubit using Landau-Zener-Stückelberg interference, *Nat. Commun.* **4**, 1401 (2013).

³⁵ L. Tarruell, D. Greif, T. Uehlinger, G. Jotzu, and T. Esslinger, Creating, moving and merging Dirac points with a Fermi gas in a tunable honeycomb lattice. *Nature* **483**, 302 (2012).

³⁶ T. Salger, C. Geckeler, S. Kling, and M. Weitz, Atomic Landau-Zener tunneling in Fourier-synthesized optical lattices. *Phys. Rev. Lett.* **99**, 190405 (2007).

³⁷ Y.-A. Chen, S. D. Huber, S. Trotzky, I. Bloch, and E. Altman, Many-body Landau-Zener dynamics in coupled one-dimensional Bose liquids. *Nat. Phys.* **7**, 61 (2011).

³⁸ B. Damski, The simplest quantum model supporting the Kibble-Zurek mechanism of topological defect production: Landau-Zener transitions from a new perspective, *Phys. Rev. Lett.* **95**, 035701 (2005).

³⁹ B. Damski and W. H. Zurek, Adiabatic-impulse approximation for avoided level crossings: From phase-transition dynamics to Landau-Zener evolutions and back again. *Phys. Rev. A* **73**, 063405 (2006).

⁴⁰ X.-Y. Xu, Y.-J. Han, K. Sun, J.-S. Xu, J.-S. Tang, C.-F. Li, and G.-C. Guo, Quantum simulation of Landau-Zener model dynamics supporting the Kibble-Zurek mechanism. *Phys. Rev. Lett.* **112**, 035701 (2014).

⁴¹ L. Wang, C. Zhou, T. Tu, H.-W. Jiang, G.-P. Guo, and G.-C. Guo, Quantum simulation of the Kibble-Zurek mechanism using a semiconductor electron charge qubit, *Phys. Rev. A* **89**, 022337 (2014).

⁴² M. Gong, X. Wen, G. Sun, D.-W. Zhang, D. Lan, Y. Zhou, Y. Fan, Y. Liu, X. Tan, H. Yu, Y. Yu, S.-L. Zhu, S. Han, and P. Wu, Simulating the Kibble-Zurek mechanism of the Ising model with a superconducting qubit system, *Sci. Rep.* **6**, 22667 (2016).

⁴³ J.-M. Cui, Y.-F. Huang, Z. Wang, D.-Y. Cao, J. Wang, W.-M. Lv, L. Luo, A. del Campo, Y.-J. Han, C.-F. Li, and G.-C. Guo, Experimental Trapped-ion Quantum Simulation of the Kibble-Zurek dynamics in momentum space, *Sci Rep.* **6**, 33381 (2016).

⁴⁴ S. M. Griffin, M. Lilienblum, K. T. Delaney, Y. Kumagai, M. Fiebig, and N. A. Spaldin, Scaling behavior and beyond equilibrium in the hexagonal manganites, *Phys. Rev. X* **2**, 041022 (2012).

⁴⁵ E. A. Novikov, Functionals and the random-force method in turbulence theory, *JETP* **20**, 1290 (1965).

⁴⁶ D. Patanè, A. Silva, L. Amico, R. Fazio, and G. E. Santoro, Adiabatic Dynamics in Open Quantum Critical Many-Body Systems, *Phys. Rev. Lett.* **101**, 175701 (2008).

⁴⁷ P. Nalbach, S. Vishveshwara, and A. A. Clerk, Quantum Kibble-Zurek physics in the presence of spatially correlated dissipation, *Phys. Rev. B* **92**, 014306 (2015).

⁴⁸ A. Dutta, A. Rahmani, and A. del Campo, Anti-Kibble-Zurek Behavior in Crossing the Quantum Critical Point of a Thermally Isolated System Driven by a Noisy Control Field, *Phys. Rev. Lett.* **117**, 080402 (2016).

⁴⁹ A. Rahmani, Dynamics of noisy quantum systems in the Heisenberg picture: Application to the stability of fractional charge, *Phys. Rev. A* **92**, 042110 (2015).

⁵⁰ K. Kim, Quantum simulation of frustrated Ising spins with trapped ions, *Nature* **465**, 590 (2010).

⁵¹ J. G. Bohnet, B. C. Sawyer, J. W. Britton, M. L. Wall, A. M. Rey, M. Foss-Feig, and J. J. Bollinger, Quantum spin dynamics and entanglement generation with hundreds of

trapped ions, *Science* **352**, 1297 (2016).

⁵² J. Simon, W. S. Bakr, R. Ma, M. E. Tai, P. M. Preiss, and M. Greiner, Quantum simulation of antiferromagnetic spin chains in an optical lattice, *Nature* **472**, 307 (2011).

⁵³ E. Lieb, T. Schultz, and D. Mattis, Two soluble models of an antiferromagnetic chain, *Ann. Phys. (N.Y.)* **16**, 407 (1961).

⁵⁴ J. E. Bunder and Ross H. McKenzie, Effect of disorder on quantum phase transitions in anisotropic XY spin chains in a transverse field, *Phys. Rev. B* **60**, 344 (1999)